Progress in Nuclear Energy 110 (2019) 301–310

Contents lists available at ScienceDirect

Progress in Nuclear Energy

journal homepage: www.elsevier.com/locate/pnucene

Development and verification of resonance elastic scattering kernel processing module in nuclear data processing code NECP-Atlas

Jialong Xu, Tiejun Zu*, Liangzhi Cao

School of Nuclear Science and Technology, Xi'an Jiaotong University, Xi'an, Shaanxi, 710049, China

ARTICLE INFO

Keywords:
Resonance elastic scattering kernel
Nuclear data processing
Doppler fuel temperature coefficient
NECP-Atlas

ABSTRACT

Some efforts have been made to exactly consider the effect of neutron up-scattering caused by thermal motion of target nuclei and resonance elastic scattering on the multi-group cross sections and scattering matrices. Firstly, the resonance elastic scattering kernel (RESK) formulations for anisotropic scattering up to any Legendre order has been adopted to represent the exact Doppler broadened energy transfer kernels. A semi-analytical integration method is applied to perform the RESK calculations. Combining with the RESK calculations, a linearization algorithm is proposed to generate the RESK interpolation tables. The RESK data can be interpolated precisely based on the interpolation tables to reduce the calculation burden. Secondly, a neutron slowing-down equation solver is developed based on the RESK instead of the conventional asymptotic scattering kernel, where the effect of neutron up-scattering on the neutron energy spectrum can be exactly considered. The accuracy of the multi-group cross sections and scattering matrices are significantly improved when the exact energy spectrum is applied for the group collapsing calculations. All the methods mentioned above have been implemented into a newly developed nuclear data processing code called NECP-Atlas. Numerical results show that the proposed methods are capable of producing accurate multi-group cross sections for downstream calculations; the fuel Doppler coefficients and eigenvalues of the real problems will be improved if the up-scattering effect is incorporated into the multi-group cross sections and matrices.

1. Introduction

Nuclear data processing plays a significant role in the design and analysis of nuclear reactors, which transforms the evaluated nuclear data into a specific format for the downstream calculation codes. NJOY (Muir and Boicourt, 2016), PREPRO (Cullen, 2017) and AMPX (Wiarda et al., 2016) et al. are widely used nuclear data processing codes.

One important function of the nuclear data processing codes is Doppler broadening the 0 K data to other desired temperatures. The thermal agitation of the target nuclides is considered in the Doppler broadening process. When a neutron at relatively low energy collides with heavy nuclides, it has a probability of gaining energy. This phenomenon is known as neutron up-scattering. Besides, some nuclides have resonance elastic scattering cross sections, which will increase the probability of neutron up-scattering. Therefore, both the scattering cross sections and energy transfer kernels should be Doppler broadened. In the widely used nuclear data processing codes, the scattering cross sections are usually Doppler broadened with an accurate method, e.g. Kernel broadening method (Cullen, 1974). However, when the energy transfer kernel is Doppler broadened, the elastic scattering cross sections are set to be a constant, ignoring the resonance phenomena of the elastic scattering cross sections. This approximation is in contradiction with the situations that many heavy nuclides have plenty of resonance peaks, which leads to large error to the Doppler broadened energy transfer kernels.

To solve the problems mentioned above, the RESK theory was proposed (Ouisloumen and Sanchez, 1991) to exactly calculate the exact Doppler broadened energy transfer kernels of different Legendre orders in a deterministic way. The researchers gave the derivation of the RESK formulae and the exact Doppler broadened energy transfer kernels can be evaluated by some integration techniques. Meanwhile, based on a stochastic method, the improved Doppler broadened rejection correction (DBRC) approach (Dagan, R. et al., 2011) was proposed to simulate the exact secondary angular and energy distributions. Since the energy transferring is caused by the collision between neutrons and nuclei, it is straightforward to simulate the collision in the Monte Carlo codes. Additionally, the RESK can be obtained by tallying the secondary angular and energy distributions calculated by Monte Carlo codes.

According to several researchers (Lee et al., 2008; Ghrayeb et al., 2011), the exact Doppler broadened energy transfer kernel shows that

* Corresponding author.
E-mail address: tiejun@xjtu.edu.cn (T. Zu).

https://doi.org/10.1016/j.pnucene.2018.10.006
Received 28 June 2018; Received in revised form 7 September 2018; Accepted 11 October 2018

the neutron up-scattering effect is strong in the resonance range. It has been proved that the exact Doppler broadened energy transfer kernel had a great impact on the Doppler coefficients and eigenvalues of the thermal spectrum reactors by several researchers (Dagan, 2005; Becker et al., 2009; Mori and Nagaya, 2009; Lee et al., 2008; Zoia et al., 2013; Ghrayeb et al., 2014; Ouisloumen et al., 2015).

Besides the Doppler broadening, another significant function of the nuclear data processing codes is to generate the multi-group cross sections and scattering matrices. The multi-group cross sections and scattering matrices are collapsed from continuous-energy data, and the weighting flux is very crucial for the generation. In the resonance range, it is a common practice to solve the neutron slowing-down equation to obtain the weighting flux. The asymptotic kernel is usually adopted to establish the neutron slowing-down equation but there are some approximations for the asymptotic kernel.

The asymptotic kernel assumes that the target nuclei are at rest, ignoring the thermal agitation of target nuclei. The assumption will lead to a problem that the resonance elastic scattering cannot have impact on the energy transfer kernels since there is no Doppler effect considered in the asymptotic kernel. Therefore, the asymptotic kernel will introduce large error to the real solution of weighting flux, which will affect the accuracy of the multi-group cross sections and scattering matrices consequently. To consider the effects of the thermal agitation of target nuclei and resonance elastic scattering on the multi-group cross sections, two kinds of methods have been proposed by several researchers:

In the first method, the multi-group cross sections calculated based on the asymptotic kernel is corrected by the correction factors (Lee et al., 2008; He et al., 2016a,b; Li et al., 2016). The correction factors are the ratio of the cross sections based on the exact Doppler broadening kernel to those based on the asymptotic kernel. The cross sections based on the exact Doppler broadening kernel are calculated by Monte Carlo codes where the DBRC approach (Dagan, R. et al., 2011) is used to consider the thermal agitation of target nuclei and the resonance elastic scattering. The multi-group scattering matrices are generated simultaneously.

In general, the Monte Carlo calculations are very time-consuming. When the group structure is relatively fine, it needs more simulated particles to obtain the converged results. Moreover, the repetitive Monte Carlo calculations are always needed since the correction factors are dependent with nuclides, temperatures, dilutions and group structures, which multiplies the computation time.

In the second method, the ultra-fine group structures (~6000 groups) are used to reduce the effect of neutron energy spectrum on the effective multi-group cross sections (Ghrayeb et al., 2014; Ouisloumen et al., 2015). In this method, the multi-group cross sections are generated based on the asymptotic kernel. The multi-group scattering matrices are generated by integrating the original formulae of the RESK. In the multi-group scattering matrices generation, the weighting flux is set to be approximately constant and it is unnecessary to obtain the weighting flux by solving the neutron slowing-down equation.

The second method cannot handle the broad group structures since the multi-group cross sections and scattering matrices can be influenced easily by the shape of weighting flux in the broad energy intervals where many strong resonance peaks are included. Similarly, for different nuclides, temperatures and group structures, the repetitive integration calculations are always needed since $\sigma_{sn}(E \rightarrow E')$ is computed from the RESK formulae in the numerical integrations of group collapsing procedures.

It is not practical to apply the first method into the nuclear data processing codes, because the computations are very time-consuming when the Monte Carlo code is used. For the second method, ultra-fine group should be used to reduce the error. However, for most of the deterministic neutronics codes, it is common to use the broad group structures. Therefore, the second method has limitations.

In this paper, some efforts have been made to get more accurate multi-group cross sections and scattering matrices. Firstly, a method to evaluate the RESK is developed and the moments of RESK at any incident energy and secondary energy can be calculated precisely in a deterministic way. A new module to process the RESK has been developed. In this module, a two-dimensional off-line RESK interpolation table is generated so that the downstream processing modules can get the RESK data accurately and efficiently. In other words, the energy transfer kernels are obtained by directly interpolating the RESK interpolation tables. Secondly, a neutron slowing-down equation solver is also developed based on the RESK to avoid the error caused by the use of asymptotic kernel. Accurate multi-group cross sections and scattering matrices can be generated based on continuous-energy spectrum taking account the neutron up-scattering effect. All the methods mentioned above have been implemented into NECP-Atlas which is a newly developed nuclear data processing code capable of processing different evaluated nuclear data files (ENDF) and generating multi-group and continuous-energy libraries (Zu and Xu, 2018).

In Section 2, the multi-group cross sections and scattering matrices generation methods considering the exact Doppler broadened energy transfer kernels are described. In Section 3, the numerical results are demonstrated. The conclusions are given in the last section.

2. Methodologies

2.1. Theory of the resonance elastic scattering kernel

The effective differential scattering cross section for neutrons of velocity v in a homogeneous medium at T Kelvin (K) is defined by the formula (Ouisloumen and Sanchez, 1991)

$$\sigma_s^T(v \rightarrow v') = \frac{1}{v}\int_{(\infty)} v_r \sigma_s(v, V \rightarrow v') M^T(V) dV \tag{1}$$

where v' is the velocity of the scattered neutron; v_r is the relative collision velocity; $\sigma_s(v,V \rightarrow v')$ is the differential scattering cross section for an individual collision event; $M^T(V)$ is the velocity spectrum of target nuclei.

The effective differential scattering cross section only depends on incident and secondary energies, E and E'. Therefore, the double differential cross section can be represented in terms of a Legendre expansion in μ_{lab},

$$\sigma_s^T(E \rightarrow E', \mu_{lab}) = \sum_{n \geq 0} (2n+1)^{-1} \sigma_{sn}^T(E \rightarrow E') P_n(\mu_{lab}) \tag{2}$$

where P_n is the Legendre polynomial of order n; μ_{lab} is the scattering angle in the laboratory frame. The energy transfer moment is given by

$$\sigma_{sn}^T(E \rightarrow E') = \int_{-1}^{1} \sigma_s^T(E \rightarrow E', \mu_{lab}) P_n(\mu_{lab}) d\mu_{lab} \tag{3}$$

By substituting Eq. (1), Eq. (3) can be rewritten as

$$\sigma_{sn}^T(E \rightarrow E') = \frac{1}{v}\int_{(\infty)} v_r \sigma_s(v_r) P_n(v, V \rightarrow E') M^T(V) dV \tag{4}$$

with

$$P_n(v, V \rightarrow E') = \int_{(\infty)} \delta\left(E' - \frac{1}{2} m v'^2\right) P_n(\mu_{lab}) P(v, V \rightarrow v') \tag{5}$$

where δ is the Dirac's delta function and $P(v,V \rightarrow v')$ is the transfer kernel for an individual event.

By assuming that $M^T(V)$ is a Maxwellian distribution, Eq. (4) reduces to the moments for the energy transfer kernel equation (Ouisloumen and Sanchez, 1991):

$$\sigma_{sn}^T(E \rightarrow E') = \frac{\beta^{5/2}}{4E} \exp(E/kT) \int_0^{\infty} t \sigma_{s,0}\left(\beta \frac{kT}{A} t^2\right) \exp(-t^2/A) \psi_n(t) dt \tag{6}$$

with

$$\beta = (A+1)/A \tag{7}$$

where t is a variable proportional to the neutron speed; $\sigma_{s,0}$ is the tabulated 0 K cross section; k is Boltzmann's constant; T is the temperature of the material; A is the ratio of the nucleus mass to the mass of the neutron.

In this paper, to calculate Eq. (6) accurately and efficiently, it takes 3 basic steps for the calculation procedure.

Firstly, it can be noticed that there is a 0 K cross section term $\sigma_{s,0}$ in Eq. (6). By the conventional linearization and resonance reconstruction methods, the energy grids of tabulated 0 K cross section are reconstructed. Based on the energy grids, the whole integral interval for the variable t is discretized into many integral subintervals. A 5-point Gauss-Legendre quadrature is applied to evaluate the integral of each subinterval. It is given by

$$\begin{aligned}\sigma_{sn}^{T}(E\to E') &= \beta^{5/2}/(4E)\cdot\exp(E/kT)\\ &\times\sum_{i=1}^{N}\int_{t_{i,\text{lower}}}^{t_{i,\text{upper}}} t_i\sigma_{s,0}(\beta kTt_i^2/A)\exp(-t_i^2/A)\psi_n(t_i)dt_i\\ &=\beta^{5/2}/(4E)\cdot\exp(E/kT)\\ &\times\sum_{i=1}^{N}\sum_{k=1}^{5} t_{i,k}\sigma_{s,0}(\beta kTt_{i,k}^2/A)\exp(-t_{i,k}^2/A)\psi_n(t_{i,k})w_k\end{aligned} \tag{8}$$

where N is the total number of the subintervals, w is the weight of Gauss-Legendre quadrature.

Furthermore, there may be a situation that the argument of the $\sigma_{s,0}$ exceeds the domain of it (i.e. $\beta kTt_{i,k}^2/A < 1\text{E-}5$ eV) since the integration boundary in Eq. (6) is from zero to infinity. Therefore, the $\sigma_{s,0}$ are assumed to vary with the $1/v$ law approximately for this situation.

Secondly, the nth order component of the angular dependence $\psi_n(t)$ in Eq. (8) is defined as

$$\begin{aligned}\psi_n(t) &= H(t_+ - t)H(t - t_-)\\ &\times\int_{\varepsilon_{\max}-t}^{t+\varepsilon_{\min}}\exp(-x^2)Q_n(x,t)dx + H(t-t_+)\\ &\times\int_{t-\varepsilon_{\min}}^{t+\varepsilon_{\min}}\exp(-x^2)Q_n(x,t)dx\end{aligned} \tag{9}$$

with

$$t_\pm = \frac{\varepsilon_{\max}\pm\varepsilon_{\min}}{2} \tag{10}$$

and

$$\varepsilon_{\max} = \sqrt{(A+1)\max(E,E')/kT} \tag{11}$$

$$\varepsilon_{\min} = \sqrt{(A+1)\min(E,E')/kT} \tag{12}$$

where H is the Heaviside step function.

The integrals in Eq. (9) are also evaluated similar to the integration methods mentioned above. The integral interval for the variable x is subdivided into equal intervals.

In particular, to enhance the efficiency of $\psi_n(t)$ calculations, the first two orders of $\psi_n(t)$ are calculated analytically (Ghrayeb et al., 2011). Combining with the analytical expressions of $Q_n(x,t)$, $\psi_0(t)$ and $\psi_1(t)$ are defined as

$$\begin{aligned}\psi_0(t) &= H(t_+ - t)H(t_- - t)\times[erf(t+\varepsilon_{\min}) - erf(\varepsilon_{\max} - t)]\\ &+H(t-t_+)[erf(t+\varepsilon_{\min}) - erf(t-\varepsilon_{\min})]\end{aligned} \tag{13}$$

$$\begin{aligned}\psi_1(t) &= \frac{1}{4\sqrt{\pi}\varepsilon_{\max}\varepsilon_{\min}}\\ &\left\{\begin{array}{l}\rho\psi_0(t) - H(t_+ - t)H(t-t_-)(g(\varepsilon_{\min},\varepsilon_{\max}) + j(\varepsilon_{\max},\varepsilon_{\min}))\\ -H(t-t_+)(g(\varepsilon_{\min},\varepsilon_{\max}) - j(\varepsilon_{\min},\varepsilon_{\max}))\end{array}\right\}\end{aligned} \tag{14}$$

with

$$\rho = \sqrt{\pi}\left\{\varepsilon_{\max}^2 + \varepsilon_{\min}^2 - 2t^2 + \frac{1}{2} - 2(\varepsilon_{\max}^2 - t^2)(\varepsilon_{\min}^2 - t^2)\right\} \tag{15}$$

and

$$g(x,y) = e^{-(t+x)^2}[t + x - 2(y^2 - t^2)(t-x)] \tag{16}$$

$$j(x,y) = e^{-(t-x)^2}[t - x - 2(y^2 - t^2)(t+x)] \tag{17}$$

Thirdly, $Q_n(x,t)$ in Eq. (9) is defined as

$$Q_n(x,t) = \frac{4}{\sqrt{\pi}}\int_0^{2\pi} P_n(\mu_{lab})P(\mu_{CM})d\phi \tag{18}$$

where

$$\mu_{CM} = \frac{1}{4x^2t^2}(A + B\cos\phi) \tag{19}$$

and

$$\mu_{lab} = \frac{1}{4x^2\varepsilon_{\max}\varepsilon_{\min}}(C + B\cos\phi) \tag{20}$$

with

$$A = (\varepsilon_{\max}^2 - x^2 - t^2)(\varepsilon_{\min}^2 - x^2 - t^2) \tag{21}$$

$$C = (\varepsilon_{\max}^2 + x^2 - t^2)(\varepsilon_{\min}^2 + x^2 - t^2) \tag{22}$$

and

$$\begin{aligned}B &= [(t+x)^2 - \varepsilon_{\max}^2][(t+x)^2 - \varepsilon_{\min}^2]\\ &\times[\varepsilon_{\max}^2 - (t-x)^2][\varepsilon_{\min}^2 - (t-x)^2]\end{aligned} \tag{23}$$

In Eq. (18), $P(\mu_{CM})$ is the angular distribution which is generally assumed to have azimuthal symmetry in the center-of-mass frame. An approximation is induced that the elastic scattering is isotropic (i.e.$P(\mu_{CM}) = 1/4\pi$) within the thermal and epi-thermal range, which matches with the descriptions in the File 4 of the ENDF for most nuclides. Based on this approximation, Eq. (18) can be evaluated analytically.

Based on these 3 basic steps mentioned above, $\sigma_{sn}^{T}(E\to E')$in Eq. (6) is evaluated precisely. The moments for the energy transfer kernels can be calculated

$$P_n^T(E\to E') = \frac{\sigma_{sn}^T(E\to E')}{\sigma_{s,0}^T(E)} \tag{24}$$

where$\sigma_{s0}^T(E)$is the Doppler broadened elastic scattering cross section at T K.

2.2. Generation of the interpolation table

In the numerical integrations of group collapsing procedure, a great number of kernels ($P_n^T(E\to E')$) are usually desired to evaluate the accurate group cross sections and scattering matrices. If each $P_n^T(E\to E')$is obtained by the methods demonstrated in Section 2.1, the total computation cost will be very large. Hence, using the interpolation tables is a compromise solution, which meets the demand of accuracy and efficiency simultaneously. More importantly, the interpolation tables can be reused to generate the group cross sections and scattering matrices with different dilutions and group structures.

For the motivation mentioned above, a linearization algorithm is proposed to generate the two-dimensional interpolation tables. The first interpolated variable is the incident energy and the second is the secondary energy. Therefore, it is crucial to obtain the proper incident energy points and the secondary energy points corresponding to each incident energy point.

A very dense incident energy grids can be adopted but it is inadvisable. On one hand, the huge number of incident energy points will increase the memory footprint and the time for looking up data. On the other hand, the shapes of energy transfer kernels vary slowly against the incident energy. From Fig. 1, it can be noticed that the shapes of 0^{th} energy transfer kernel at 4.5 eV, 5.0 eV, 5.5 eV and 6.0 eV change slowly, which means several energy points can represent the variation

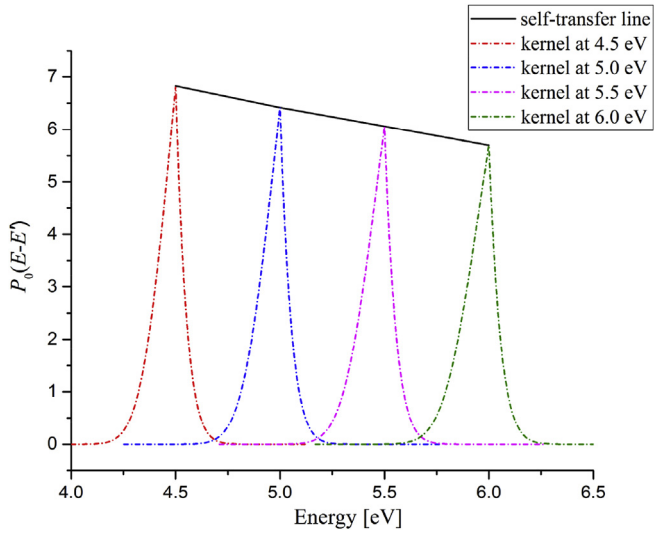

Fig. 1. The 0th energy transfer kernels from 4.5 eV to 6.0 eV.

trends of the transfer kernel. It is unnecessary to set huge amount of incident energy points.

In Fig. 1, the black solid line is constructed by linking the self-transfer points at the 4 energy points mentioned above. It can be noticed that the black solid line vary smoothly. So a deduction is made that the kernels change slowly when the self-transfer points vary smoothly. As a result, by assuming that the shapes of energy transfer kernels are closely dependent with the values of self-transfer points, the energy transfer kernels will be interpolated with the special projection interpolation scheme (Muir and Boicourt, 2016) if the self-transfer points are linearly interpolated. Therefore, a linearization method is proposed to obtain the incident energy grids. The principle of the algorithm is to keep the 0th self-transfer points (i.e.$P_0^T(E \to E')$) linear within any incident energy interval under the given criteria. Through this linearization, the incident grids for different nuclides and temperatures are reconstructed. The RESK calculations described in Section 2.1 are only performed at the energy points of the incident energy grids. The linearization algorithm is decomposed into several steps and shown in Fig. 2.

At each reconstructed incident energy, the moments of energy transfer kernels for the different orders are linearized simultaneously on a single unionized grid by the conventional interval-halving techniques (Cullen, 2010). It ensures that all orders of the moments are reconstructed smoothly. Meanwhile, the moments of energy transfer kernels for the different orders are interpolated simultaneously once the interpolation interval is found.

An unassigned reaction type number in ENDF-6 format is applied to store and output the interpolation table of the RESK data and the "MF6 MT300" reaction type is defined. The data structure in ENDF-6 format is proposed and the data structure is defined in Fig. 3.where HEAD, TAB2, TAB1, LIST are the standard types of records; ZA, AWR are the standard material charge and mass parameters; NL is the maximum Legendre order number of this table; E' is the secondary energy; P_0 indicates the 0th moment of energy transfer kernel and P_1 represents the 1st moment of energy transfer kernel, and so on.

After the processing, the data will be output into derived files which are the "point-ENDF" (PENDF) files. The reusable PENDF files can be used for generating the different multi-group cross sections and scattering matrices faced with the different requirements of dilutions and energy group structures.

2.3. Solving the neutron slowing-down equation

Generating the multi-group cross sections and scattering matrices is an important function of nuclear data processing codes. Accurate weighting flux is needed to evaluate the multi-group cross sections and scattering matrices.

To obtain the reliable self-shielded weighting flux in the resonance range, the 0-dimensional neutron slowing-down equation is solved

$$\sum_{i=1}^{N} \Sigma_{t,i}(E)\phi(E) = \sum_{i=1}^{N} \int_0^{\infty} P_i(E' \to E)\Sigma_{s,i}(E')\phi(E')dE' \tag{25}$$

where $\phi(E)$ is the neutron flux, i is the nuclide index; N is the total number of nuclide types; $\Sigma_{t,i}(E)$ is the macro total cross section; $\Sigma_{s,i}(E')$ is the macro elastic scattering cross section; $P_i(E' \to E)$ represents the 0th energy transfer kernel. In the following equations, the superscript of temperature T for each arguments will be omitted.

The equation is solved from the high energy to low energy point by point. In this paper, the energy grids for solving are generated by stacking the energy points of tabular cross sections from each nuclide. Based on the energy grids, Eq. (25) can be discretized,

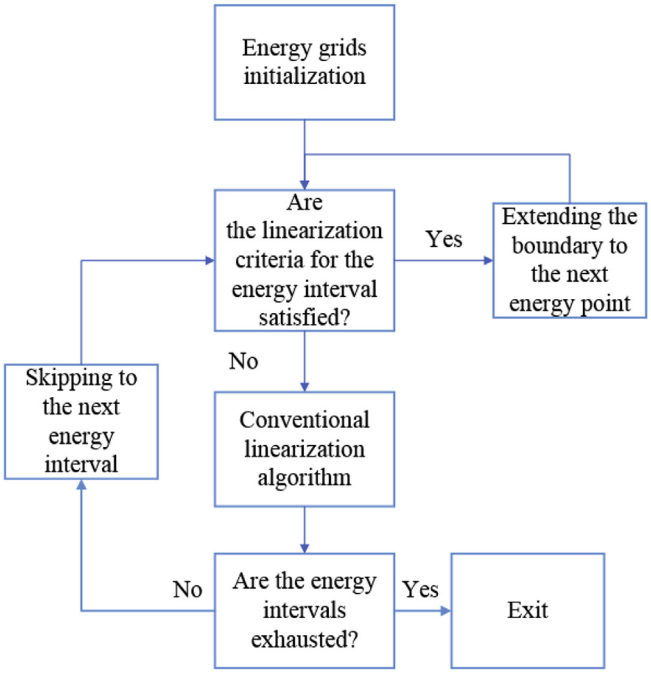

Fig. 2. The schematic diagram of the modified linearization algorithm.

1) Initializing the incident energy grids. In general, it is obtained from the energy grids of the tabular cross section at 0 K.
2) Checking whether the linearization criteria are satisfied for the energy interval.
3) If the criteria is not met, the conventional interval-halving technique which is usually used in many processing code will be performed. Then, skipping to the next energy interval and Step 2 is repeated unless the energy intervals are exhausted.
4) If the criteria is met, extending the energy interval boundary to the next energy point and Step 2 is repeated.

[MAT, 6, MT/ ZA, AWR, NL, 0, 0, 0, 0] HEAD
[MAT, 6, MT/ T, 0.0, 0, 0, NR, NE/ E_{int}] TAB2
[MAT, 6, MT/ 0.0, E_1.0, 0, 0, NRP, NEP/ $E' / P_0(E_1 \to E')$] TAB1
[MAT, 6, MT/ 0.0, 0.0, 0, 0, NW, 0/
$P_1(E_1 \to E_1'), P_1(E_1 \to E_2'),$ --------, $P_1(E_1 \to E_{NW}')$] LIST
<Repeat the LIST structure for all the NL-1 orders>
<Repeat the TAB1 structure for all the NE incident energies>

Fig. 3. The data structure of the "MF6 MT300" reaction type.

$$\sum_{i=1}^{N}\Sigma_{t,i}(E)\phi(E)=\sum_{i=1}^{N}\sum_{j=1}^{M}\int_{\Delta E'_j}P_i(E'_j\rightarrow E)\Sigma_{s,i}(E'_j)\phi(E'_j)dE'_j \tag{26}$$

where M is the total number of energy subintervals.

The cross sections are obtained directly from the PENDF using the linear-linear interpolation scheme since they are linearized. Meanwhile, based on the special projection interpolation scheme and the interpolation tables mentioned in Section 2.2, the energy transfer kernels are obtained from PENDF as well. And it is assumed that the flux in each subinterval is linearly dependent. Therefore, the algebraic precision of the integral in each subinterval is 3 and 2-point Gauss-Legendre quadrature is accurate enough to evaluate the integrals in Eq. (26). It can be written as

$$\sum_{i=1}^{N}\Sigma_{t,i}(E)\phi(E)=\sum_{i=1}^{N}\sum_{j=1}^{M}\sum_{k=1}^{2}P_i(E'_{j,k}\rightarrow E)\Sigma_{s,i}(E'_{j,k})\phi(E'_{j,k})w_k \tag{27}$$

where

$$P_i(E'_{j,k}\rightarrow E)=[x_k\cdot(P_i(E'_{j2}\rightarrow E)-P_i(E'_{j1}\rightarrow E))+P_i(E'_{j2}\rightarrow E)+P_i(E'_{j1}\rightarrow E)]\cdot 0.5 \tag{28}$$

$$\Sigma_{s,i}(E'_{j,k})=[x_k\cdot(\Sigma_{s,i}(E'_{j2})-\Sigma_{s,i}(E'_{j1}))+\Sigma_{s,i}(E'_{j2})+\Sigma_{s,i}(E'_{j1})]\cdot 0.5 \tag{29}$$

$$\phi(E'_{j,k})=[x_k\cdot(\phi(E'_{j2})-\phi(E'_{j1}))+\phi(E'_{j2})+\phi(E'_{j1})]\cdot 0.5 \tag{30}$$

where x_k and w_k are the node and weight of Gauss-Legendre quadrature for point k respectively; $E'_{j1}$and$E'_{j2}$are the lower and upper boundaries of the energy interval j.

Since the neutron up-scattering effects are considered in the neutron slowing-down equation, it is necessary to solve the neutron slowing-down equation iteratively. The Gauss-Seidel iteration strategy is adopted to solve the neutron slowing-down equation. Eq. (27) combined with Eq. (28)-Eq. (30) can be written as a system of linear equations,

$$\begin{cases}\sum_{i=1}^{N}a_{11,i}\phi(E_1)+a_{12,i}\phi(E_2)+\cdots+a_{1n,i}\phi(E_n)=\sum_{i=1}^{N}b_{1,i}\\ \sum_{i=1}^{N}a_{21,i}\phi(E_1)+a_{22,i}\phi(E_2)+\cdots+a_{2n,i}\phi(E_n)=\sum_{i=1}^{N}b_{2,i}\\ \cdots\cdots\\ \sum_{i=1}^{N}a_{n1,i}\phi(E_1)+a_{n2,i}\phi(E_2)+\cdots+a_{nn,i}\phi(E_n)=\sum_{i=1}^{N}b_{3,i}\end{cases} \tag{31}$$

It is well known that the initial values near the real solution can help the iteration converge. It is reasonable to consider that the flux solved based on the asymptotic kernel is near the real solution. Based on the asymptotic kernel, the hyper-fine method (Leszczynski, 1987) is adopted to solve the neutron slowing-down equation efficiently to get the initial hyper-fine group flux in this paper. In the group collapsing calculations, the continuous-energy flux is usually used rather than hyper-fine group flux. As a result, an assumption is made that the average value of a hyper-fine group flux is equal to the middle point flux of this hyper-fine group. It is given by

$$\phi(E_{\mathrm{mid}})\approx\frac{\phi_g}{\Delta E_g} \tag{32}$$

where E_{mid} is the middle energy of the hyper-fine group g; ϕ_g is the hyper-fine group flux; ΔE_g is the energy width of the hyper-fine group.

In summary, the whole solving procedure is decomposed into several steps (See Fig. 4).

Thus, the weighting flux with neutron up-scattering effects considered is obtained and the multi-group cross sections and scattering matrices are generated.

2.4. Multi-group cross section and matrix generation

Based on the traditional group collapsing methods, the multi-group cross sections and scattering matrices are generated. The multi-group

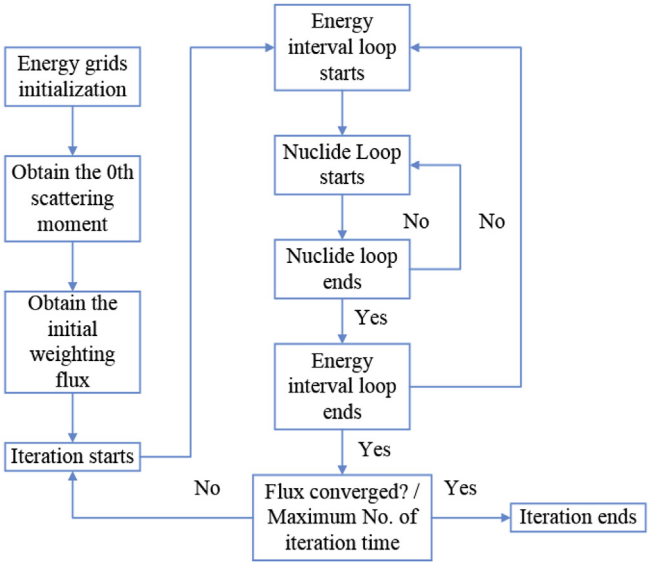

Fig. 4. The schematic diagram of the method for solving the neutron slowing-down equation.

1) The energy grids are initialized and the neutron slowing-down equation is discretized.
2) Based on the energy grids defined in Step 1, the point-point 0^{th} energy transfer moments are interpolated using the RESK interpolation tables.
3) The initial weighting flux is obtained by solving the neutron slowing-down equation using the hyper-fine group method.
4) According to Eq. (27), the scattering sources of each energy interval are evaluated by summing the scattering source of each nuclide. There may be 3 different types of energy transfer kernels according to different nuclides:
   a) The energy transfer kernel for the nuclide is based on the RESK.
   b) The energy transfer kernel for the nuclide is based on the asymptotic kernel. The scattering source is calculated based on the analytical expression approximating that the flux and cross sections in the interval are both linear.
   c) If the energy intervals for scattering source calculations exceed the top boundary, the scattering kernels for the all nuclides are set to be the asymptotic kernel.
5) The iteration will exit if the point flux converges or the maximum number of iterations is reached.

cross sections and transfer matrices are represented by,

$$\sigma_{x,g}^{n}=\frac{\int_{\Delta E_g}\sigma_x(E)\phi_n(E)dE}{\int_{\Delta E_g}\phi_n(E)dE} \tag{33}$$

$$\sigma_{sn}^{g\rightarrow g'}=\frac{\int_{\Delta E_g}\int_{\Delta E_{g'}}\sigma_{sn}(E\rightarrow E')\phi_n(E)dE'dE}{\int_{\Delta E_g}\phi_n(E)dE}=\frac{\int_{\Delta E_g}\int_{\Delta E_{g'}}\sigma_s(E)P_n(E\rightarrow E')\phi_n(E)dE'dE}{\int_{\Delta E_g}\phi_n(E)dE} \tag{34}$$

where $\sigma_x(E)$ is the continuous-energy cross section of reaction x; $\phi_n(E)$ is the continuous-energy weighting flux of order n; $P_n(E\rightarrow E')$ is the energy transfer kernel.

In Eq. (34), $P_n(E\rightarrow E')$ for "MF6 MT300" will be interpolated from the RESK interpolation tables. The trapezoid integration scheme is adopted for the secondary group collapsing since the data is linear. The other multi-group cross sections and scattering matrices are generated by the conventional methods (Macfarlane and Kahler, 2010) including processing the data in File 3, File 4, File 5 and File 6 of the ENDF (Trkov et al., 2018).

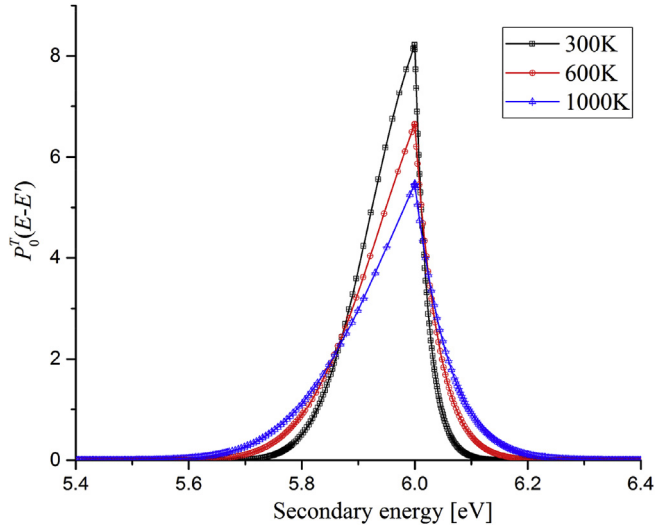

Fig. 5. The transfer kernel of ^{235}U at various temperatures for neutrons of energy 6.0 eV.

3. Numerical results

The methods described in Section 2 are developed and implemented into NECP-Atlas. NECP-Atlas is a newly developed nuclear data processing code written in the language of FORTRAN 2008 with object-oriented method. In order to research more accurate nuclear processing methods conveniently, different processing functions are encapsulated in different modules. All of the data processed by NECP-Atlas is based on the ENDF/B-VII.1.

3.1. Numerical examples of RESK

Fig. 5 and Fig. 6 show the kernels of ^{235}U at 6.0 eV and 6.8 eV. The kernels of ^{238}U at 6.52 eV and 7.2 eV are displayed in Fig. 7 and Fig. 8. The results of ^{238}Pu at 18.45 eV and 19.4 eV are also presented in Fig. 9 and Fig. 10. All of the results are calculated at 3 different temperatures which are 300 K, 600 K and 1000 K, respectively. The results also show that the kernels are effectively linearized. The squares, circles and triangles in the figures are the reconstructed points by the linearization algorithm.

Meanwhile, the first six Legendre moments of the kernels for ^{235}U at

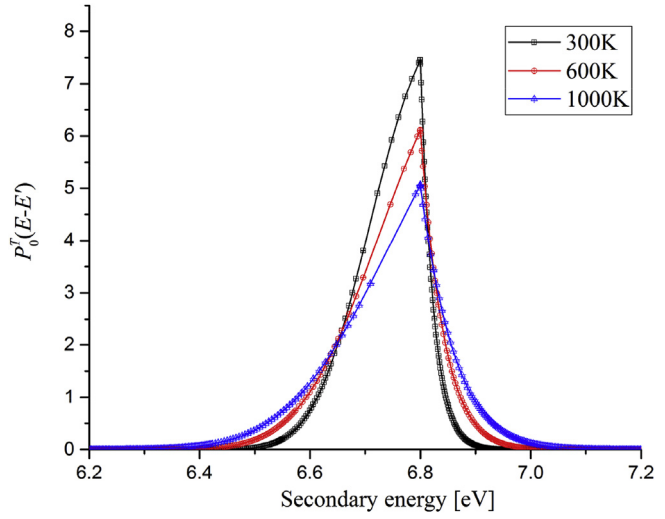

Fig. 6. The transfer kernel of ^{235}U at various temperatures for neutrons of energy 6.8 eV.

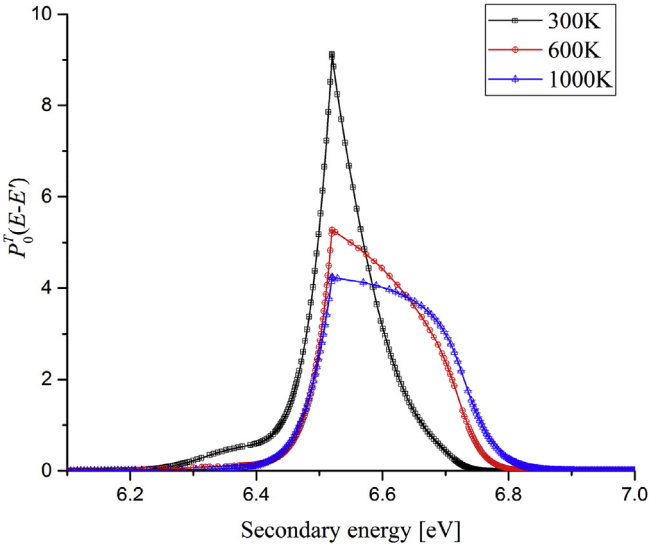

Fig. 7. The transfer kernel of ^{238}U at various temperatures for neutrons of energy 6.52 eV.

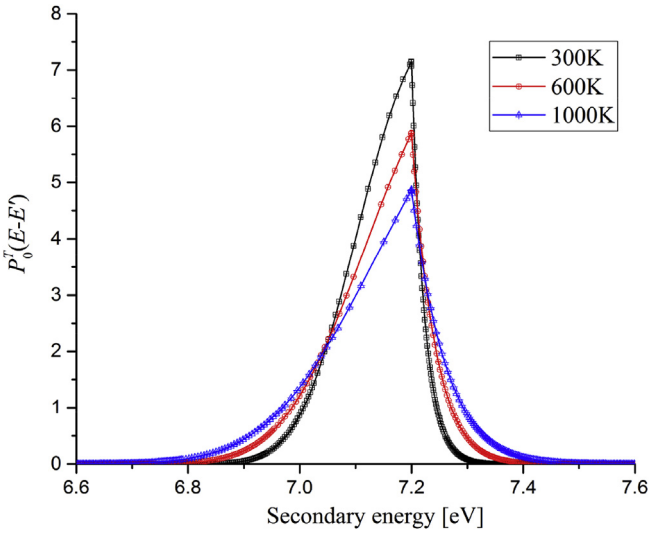

Fig. 8. The transfer kernel of ^{238}U at various temperatures for neutrons of energy 7.2 eV.

6.0 eV are shown in Fig. 11. Fig. 12 displays the first six Legendre moments of the kernels for ^{238}U at 6.52 eV and the first six Legendre moments of the kernels for ^{238}Pu at 18.45 eV are presented in Fig. 13. All the kernels are evaluated at 1000 K.

3.2. Performance of the interpolation tables

The interpolation tables at 900 K are generated for ^{238}U, ^{239}Pu and ^{242}Pu and they are used for interpolating the moments of 0^{th} kernel.

First, the incident energy grid of the interpolation table for ^{238}U is generated and shown in Fig. 14 (1E-5 eV to 100 eV) and Fig. 15 (15 eV–25 eV). It can be seen that the energy points are much closer around the resonance peaks. From 1E-5 eV to 100 eV, there are 870 points making up the incident energy grid of the interpolation table. Around 20.87 eV (the second s-wave resonance of ^{238}U), there are 172 points making up the incident energy grid of the interpolation table. The incident energy grids are optimized according to positions where the resonance peaks are located.

Then, by setting the calculated kernels as references, the kernel of ^{238}U at 6.52 eV, the kernel of ^{239}Pu at 0.15 eV and the kernel of ^{242}Pu at

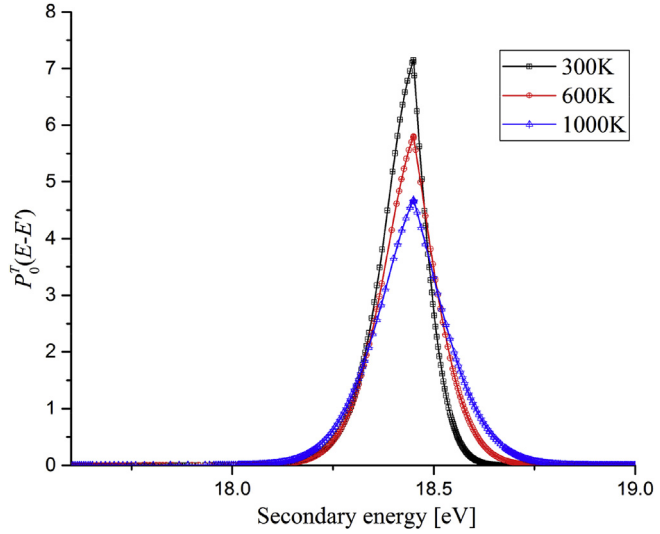

Fig. 9. The transfer kernel of ^{238}Pu at various temperatures for neutrons of energy 18.45 eV.

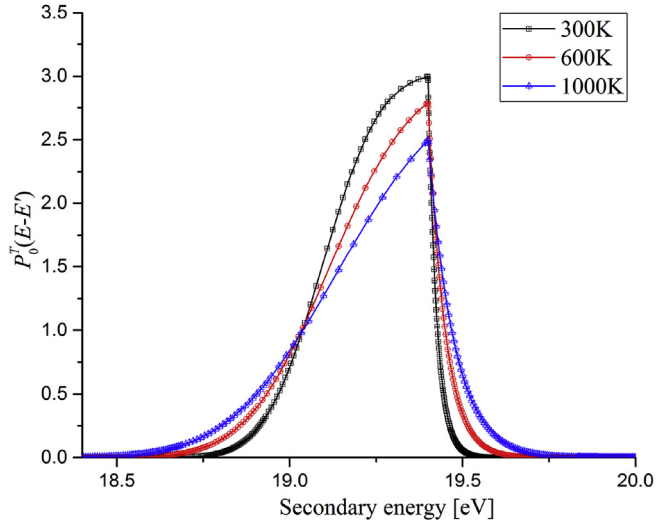

Fig. 10. The transfer kernel of ^{238}Pu at various temperatures for neutrons of energy 19.4 eV.

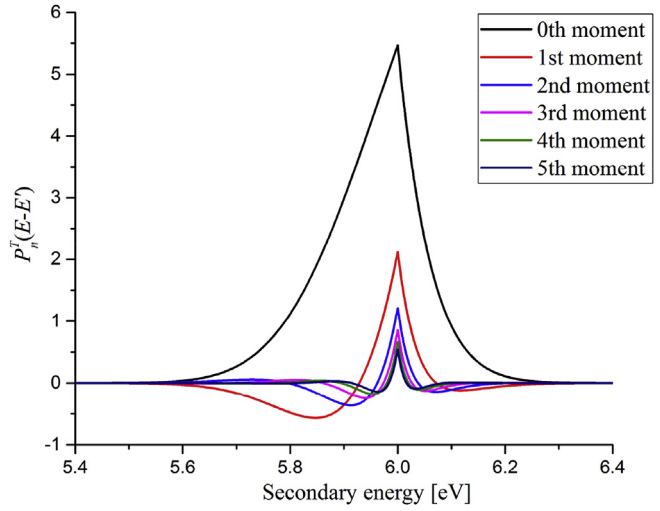

Fig. 11. First six Legendre moments of the transfer kernel for ^{235}U for neutrons of energy 6.5 eV at 1000 K.

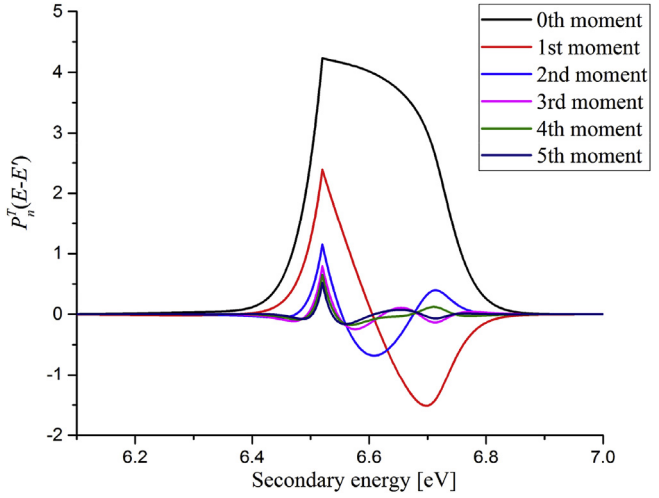

Fig. 12. First six Legendre moments of the transfer kernel for ^{238}U for neutrons of energy 6.52 eV at 1000 K.

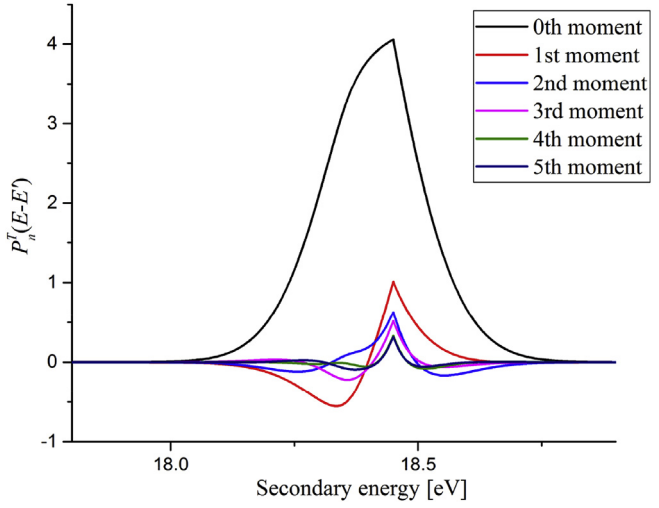

Fig. 13. First six Legendre moments of the transfer kernel for ^{238}Pu for neutrons of energy 18.45 eV at 1000 K.

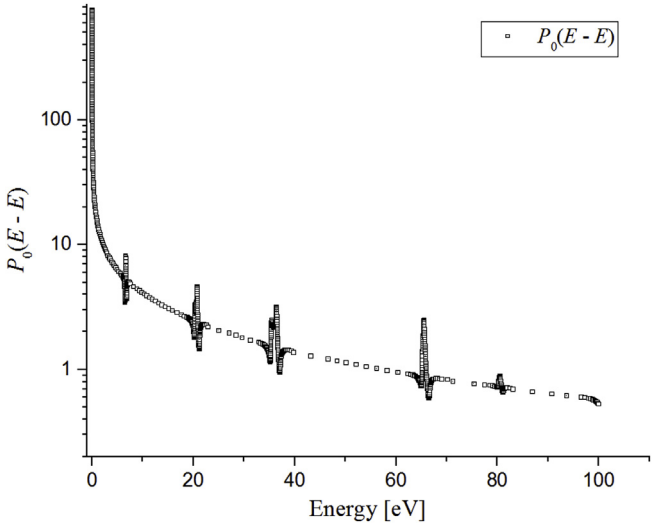

Fig. 14. Incident energy grid (1E-5 eV - 100 eV) for ^{238}U at 900 K.

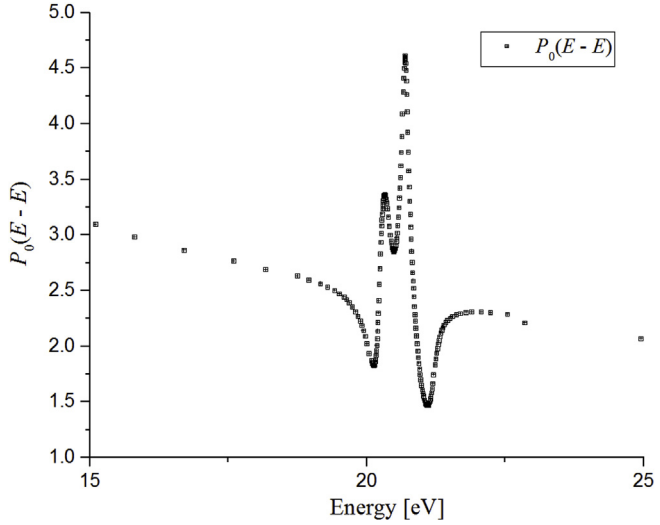

Fig. 15. Incident energy grid (15 eV - 25 eV) for ^{238}U at 900 K.

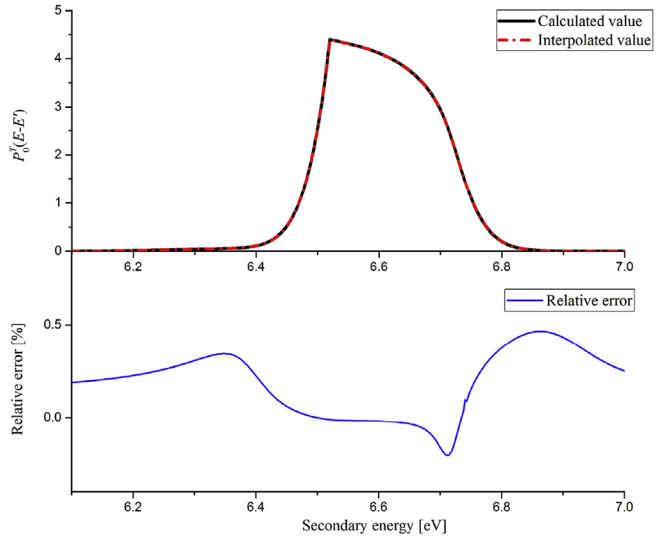

Fig. 16. The comparison of the transfer kernel of ^{238}U at 6.52 eV.

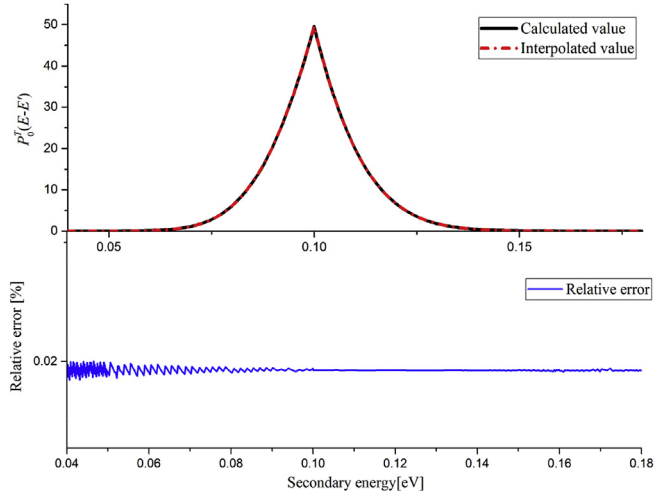

Fig. 17. The comparison of the transfer kernel of ^{239}U at 0.15 eV.

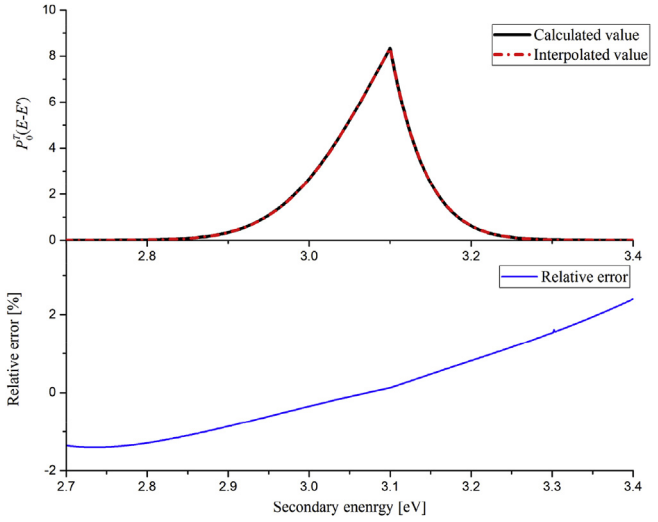

Fig. 18. The comparison of the transfer kernel of ^{242}Pu at 2.63 eV.

2.63 eV are compared. The comparison results between interpolated values and calculated values are shown in Fig. 16, Fig. 17 and Fig. 18, respectively. The interpolated values match well with the calculated values for ^{238}U, ^{239}Pu and ^{242}Pu. The maximum errors are 0.47%, 0.08% and 2.41%, respectively.

3.3. Performance of the neutron slowing-down equation solver considering the neutron up-scattering

Two infinite homogeneous systems at 900 K consisting ^{238}U and ^{1}H are designed. The background cross sections of ^{238}U in the system are 100 b and 1000 b, respectively. The neutron slowing-down equation is solved from 100 eV to 0.1 eV based on the RESK and the asymptotic kernel, respectively. The flux and absorption reaction rates based on the different kernels are displayed. Figs. 19 and 20 show the results around the ^{238}U 36.68 eV resonance for different dilutions.

The shapes of the neutron flux and absorption rates change greatly around the resonance peak due to the difference of the kernels. With the RESK, the absorption reaction rates increase more when the dilute cross sections decrease. . It needs 5.58 s to perform the whole solving procedure including one time of initialization and two times of flux

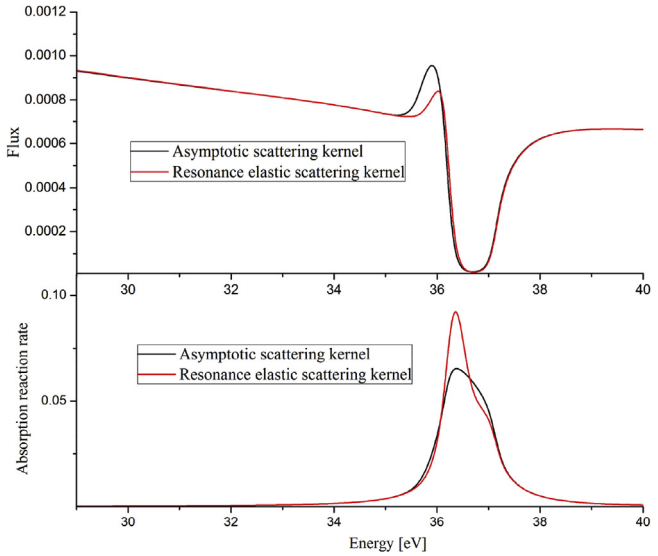

Fig. 19. Neutron spectrum and absorption reaction rate at background cross section 100 b (^{238}U resonance at 36.68 eV).

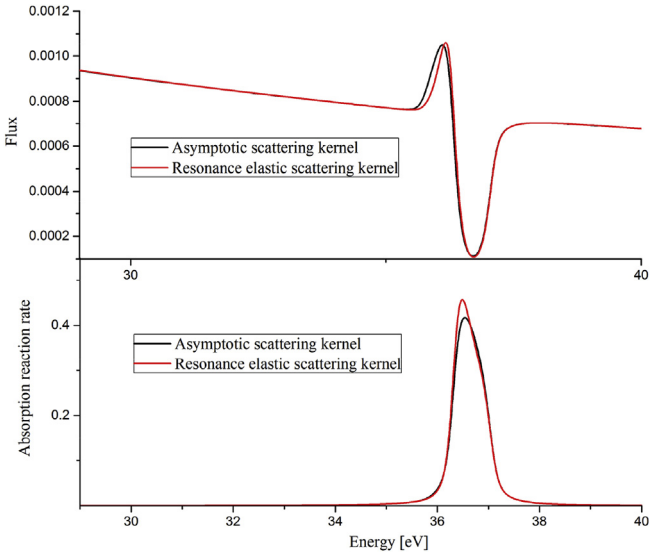

Fig. 20. Neutron spectrum and absorption rate at background cross section 1000 b (^{238}U resonance at 36.68 eV).

Table 1
Eigenvalues and fuel temperature coefficients for the Mosteller UOX fuel benchmark.

UO_2 (wt. %)	*k* (asymptotic kernel)			*k* (RESK)			FTC diff (%)
	HZP	HFP	FTC	HZP	HFP	FTC	
0.71	0.66656	0.66076	−4.39	0.66631	0.65991	−4.85	−10.5
1.60	0.96140	0.95291	−3.09	0.96105	0.95169	−3.41	−10.4
2.40	1.09918	1.08953	−2.69	1.09879	1.08816	−2.96	−10.3
3.10	1.17679	1.16653	−2.49	1.17639	1.16509	−2.75	−10.3
3.90	1.23902	1.22831	−2.35	1.23861	1.22683	−2.58	−10.2
4.50	1.27416	1.26321	−2.27	1.27376	1.26171	−2.50	−10.2
5.00	1.29831	1.28719	−2.22	1.29790	1.28569	−2.44	−10.0

Table 2
Eigenvalues and fuel temperature coefficients for the Mosteller Reactor-Recycle MOX fuel benchmark.

PuO_2 (wt. %)	*k* (asymptotic kernel)			*k* (RESK)			FTC diff (%)
	HZP	HFP	FTC	HZP	HFP	FTC	
1.00	0.94611	0.93574	−3.90	0.94554	0.93420	−4.28	−9.6
2.00	1.02198	1.01053	−3.70	1.02130	1.00883	−4.03	−9.2
4.00	1.07645	1.06435	−3.52	1.07582	1.06268	−3.83	−8.8
6.00	1.10585	1.09343	−3.42	1.10517	1.09177	−3.70	−8.1
8.00	1.13016	1.11766	−3.30	1.12945	1.11600	−3.56	−7.8

Table 3
Eigenvalues and fuel temperature coefficients for the Mosteller Weapon-Grade MOX fuel benchmark.

PuO_2 (wt. %)	*k* (asymptotic kernel)			*k* (RESK)			FTC diff (%)
	HZP	HFP	FTC	HZP	HFP	FTC	
1.00	1.09023	1.07993	−2.92	1.08968	1.07837	−3.21	−10.0
2.00	1.18164	1.16969	−2.88	1.18096	1.16791	−3.15	−9.4
4.00	1.25102	1.23801	−2.80	1.25024	1.23611	−3.05	−8.8
6.00	1.28781	1.27453	−2.70	1.28701	1.27264	−2.92	−8.4

calculations. For one temperature, only one time of initialization is required for all flux calculations, which takes 5.42 s. The flux calculations take a little computation time. The computation platform is Intel i7-7700 @ 3.60 GHz.

3.4. Verifications of Doppler benchmark calculation

The Mosteller Doppler benchmark (Mosteller, 2006) is calculated by DRAGON5 (Marleau et al., 2014) based on the EPRI-CPM 69 group structure multi-group libraries in WIMS-D4 format generated by NECP-Atlas. Two kinds of multi-group libraries are generated considering the RESK and the asymptotic kernel, respectively. For the libraries with RESK considered, the RESK is applied to all the heavy nuclides.

The results of eigenvalue and Doppler fuel temperature coefficients (FTC) at 600 K (HZP) and 900 K (HFP) based on two different multi-group libraries are compared and summarized in Tables 1-3.

The eigenvalues and Doppler fuel coefficients are influenced greatly as a result of the rising of the absorption reaction rates. About 8–10% improvement of the Doppler fuel coefficients is made based on the RESK and the eigenvalues are overestimated about 100–200 pcm at HFP in the Mosteller Doppler benchmark calculations. The results in Table 1 match with the observation of other researchers (Lee et al., 2008; Ouisloumen et al., 2015). The results in Tables 2 and 3 also agree with conclusions of other researchers (Ghrayeb, S. Z. et al., 2014; Ouisloumen et al., 2015).

4. Conclusion

Several efforts have been made to get more accurate multi-group cross sections and scattering matrices. Firstly, a semi-analytical integration method is adopted to evaluate the RESK precisely. An algorithm combining the RESK calculation is proposed to generate a two-dimensional interpolation table to obtain the RESK correctly and efficiently. The results shows that the incident energy grids of interpolation tables can be optimized and the interpolated values can match with the calculated values. Secondly, a neutron slowing-down equation solver is developed based on the RESK to provide accurate weighting flux for the multi-group collapsing calculations, which can avoid the error caused by the asymptotic kernel. The multi-group cross sections or scattering matrices for arbitrary group structures can be generated precisely and efficiently. The proposed methods have been implemented into a newly developed nuclear data processing code NECP-Atlas. The numerical tests show that the results of Mosteller Doppler benchmark are improved when the multi-group cross sections generated by NECP-Atlas are used in the calculations.

It can be observed that the eigenvalues of all cases decrease when the RESK is applied. The reason is that more neutrons are scattered into resonance peaks and the absorption reaction rates increase. It is worth noting that the conventional reactor analysis methods based on the asymptotic kernel underestimate another key parameter of reactors (i.e. fuel temperature coefficients). For example, in the control rod ejection accidents, the ejection leads that the core temperature rise. Therefore, the negative feedback effect based on the RESK is more strong compared with that based on the asymptotic kernel. Similarly, for other situations where temperature changes significantly, it is crucial to take into account the impact caused by the RESK.

Acknowledgement

This work was supported by The National Natural Science Foundation of China (No. 11605128), Science Challenge Program (No. JCKY2016212A502) and Fundamental Research Funds for the Central University (xjj2015047).

References

Becker, B., Dagan, R., Lohnert, G., 2009. Proof and implementation of the stochastic formula for ideal gas, energy dependent scattering kernel. Ann. Nucl. Energy 36, 470–474.

Cullen, D.E., 1974. Program SIGMA1 (Version 74-1). UCID-16426, Lawrence Livermore Laboratory Report, January 1974.

Cullen, D.E., 2010. Nuclear Data Preparation, Volume 1 of Handbook of Nuclear Engineering. pp. 319–350.

Cullen, D.E., 2017. PREPRO 2017, 2017. ENDF/B Preprocessing Codes (ENDF/B-VII or Proposed VIII Tested). IAEA-NDS-39, Rev.17 2017 International Atomic Energy Agency, Vienna, Austria.

Dagan, R., et al., 2011. Modelling a resonance dependent angular distribution via DBRC in Monte Carlo Codes. J. Kor. Phys. Soc. 59 (2), 983–986.

Dagan, R., 2005. On the use of S(α, β) tables for nuclides with well pronounced resonances. Ann. Nucl. Energy 32, 367–377.

Ghrayeb, S.Z., et al., 2014. Multi-group formulation of the temperature-dependent resonance scattering model and its impact on reactor core parameters. Ann. Nucl. Energy 63, 751–762.

Ghrayeb, S.Z., Ouisloumen, M., Ougouag, A.M., Ivanov, K.N., 2011. Deterministic modeling of higher angular moments of resonant neutron scattering. Ann. Nucl. Energy 38, 2291–2297.

He, Q., et al., 2016a. Resonance calculation of fluoride salt-cooled high-temperature reactor based on subgroup method. Ann. Nucl. Energy 88, 204–217.

He, Q., et al., 2016b. Neutron up-scattering effect in refined energy group structure. In: Proceedings of the 2016 24th International Conference on Nuclear Engineering ICONE24, Charlotte, North Carolina, USA, JUNE 26-30, 2016.

Lee, D., Smith, K., Rhodes, J., 2008. The impact of 238U resonance elastic scattering approximations on thermal reactor Doppler reactivity. In: International Conference on Reactor Physics, Nuclear Power: a Sustainable Resource, (Interlaken, Switzerland), September 14–19, 2008.

Leszczynski, F., 1987. Neutron resonance treatment with details in space and energy for pin cells and rod clusters. Ann. Nucl. Energy 14, 589–601.

Li, Y., et al., 2016. Resonance elastic scattering and interference effects treatments in subgroup method. Nuclear Engineering and Technology 48, 339–350.

Macfarlane, R.E., Kahler, A.C., 2010. Methods for processing ENDF/B-VII with NJOY. Nucl. Data Sheets 111, 2739–2890.

Marleau, G., Hébert, A., Roy, R., 2014. A User Guide for Dragon Version 5, Technical Report IGE 335 2014 École Polytechniquue de Montréal.

Mori, T., Nagaya, Y., 2009. Comparison of resonance elastic scattering models newly implemented in MVP continuous-energy Monte Carlo code. J. Nucl. Sci. Technol. 46 (8), 793–798.

Mosteller, R.D., 2006. Computational Benchmark for the Doppler Reactivity Defect, Tech. Rep. LA-UR-06-2968 2006 Los Alamos National Laboratory.

Muir, W.D., Boicourt, R.M., et al., 2016. The NJOY Nuclear Data Processing System, Version 2016. LA-UR- 17-20093 2016 Los Alamos National Laboratory, Los Alamos, USA.

Ouisloumen, M., Ougouag, A.M., Ghrayeb, S.Z., 2015. Anisotropic elastic resonance scattering model for the neutron transport equation. Nucl. Sci. Eng. 179, 59–84.

Ouisloumen, M., Sanchez, R., 1991. A model for neutron scattering off heavy isotopes that accounts for thermal agitation effects. Nucl. Sci. Eng. 107, 189–200.

Trkov, A., Herman, M., Brown, D.A., 2018. ENDF-6 Formats, Manual Data Formats and Procedures for the Evaluated Nuclear Data Files ENDF/B-VI, ENDF/B-VII and ENDF/B-VIII. BNL-203218-2018-INRE, National Nuclear Data Center 2018 Brookhaven National Laboratory.

Wiarda, D., Dunn, M.E., Greene, N.M., Williams, M.L., Celik, C., Petrie, L.M., 2016. AMPX-6: a Modular Code System for Processing ENDF/B. Oak Ridge National Laboratory, USA ORNL/TM-2016/43.

Zoia, A., Brun, E., Jouanne, C., Malvagi, F., 2013. Doppler broadening of neutron elastic scattering kernel in TRIPOLI-4. Ann. Nucl. Energy 54, 218–226.

Zu, T., Xu, J., et al., 2018. Development and validation of nuclear data processing code NECP-Atlas. Atomic Energy Sci. Technol. 52, 1–6 in Chinese.